

RESEARCH ARTICLE

10.1002/2015WR017906

Key Points:

- Hand-held surface velocity radars allow safe and rapid gauging of high flows
- Gauging error is within 10% in low roughness channels
- Surface velocity radars can be used to extend the validity of rating curves

Correspondence to:

M. Welber,
mwelber@uwo.ca

Citation:

Welber, M., J. Le Coz, J. B. Laronne, G. Zolezzi, D. Zamler, G. Dramais, A. Hauet, and M. Salvaro (2016), Field assessment of noncontact stream gauging using portable surface velocity radars (SVR), *Water Resour. Res.*, 52, doi:10.1002/2015WR017906.

Received 27 JUL 2015

Accepted 23 JAN 2016

Accepted article online 28 JAN 2016

Field assessment of noncontact stream gauging using portable surface velocity radars (SVR)

Matilde Welber¹, Jérôme Le Coz², Jonathan B. Laronne³, Guido Zolezzi¹, Daniel Zamler³, Guillaume Dramais², Alexandre Hauet⁴, and Martino Salvaro¹

¹Department of Civil, Environmental and Mechanical Engineering, University of Trento, Trento, Italy, ²Irstea, UR HHLY, Hydrology-Hydraulics, Villeurbanne, France, ³Department of Geography and Environmental Development, Ben Gurion University of the Negev, Beer Sheva, Israel, ⁴Electricité de France, DTG, Grenoble, France

Abstract The applicability of a portable, commercially available surface velocity radar (SVR) for noncontact stream gauging was evaluated through a series of field-scale experiments carried out in a variety of sites and deployment conditions. Comparisons with various concurrent techniques showed acceptable agreement with velocity profiles, with larger uncertainties close to the banks. In addition to discharge error sources shared with intrusive velocity-area techniques, SVR discharge estimates are affected by flood-induced changes in the bed profile and by the selection of a depth-averaged to surface velocity ratio, or velocity coefficient (α). Cross-sectional averaged velocity coefficients showed smaller fluctuations and closer agreement with theoretical values than those computed on individual verticals, especially in channels with high relative roughness. Our findings confirm that $\alpha = 0.85$ is a valid default value, with a preferred site-specific calibration to avoid underestimation of discharge in very smooth channels (relative roughness ~ 0.001) and overestimation in very rough channels (relative roughness > 0.05). Theoretically derived and site-calibrated values of α also give accurate SVR-based discharge estimates (within 10%) for low and intermediate roughness flows (relative roughness 0.001 to 0.05). Moreover, discharge uncertainty does not exceed 10% even for a limited number of SVR positions along the cross section (particularly advantageous to gauge unsteady flood flows and very large floods), thereby extending the range of validity of rating curves.

1. Introduction

Techniques for the determination of water discharge in rivers usually rely on mechanical, electromagnetic or acoustic velocimetry instrumentation requiring contact with the flow. As a consequence, safety and logistic issues limit the applicability of conventional methods to gauge high flows. Noncontact methods based on remote sensing of water surface velocity using Doppler radars or image sequence analysis have been developed in the past two decades. In the recent few years, handheld Surface Velocity Radars (SVRs) have been increasingly used by some national hydrological services, e.g., in France, for flood stream gauging operations. Due to their convenience and suitability for flood conditions, SVRs have begun to provide valuable discharge data in upper-end sections of rating curves that had previously been impossible to obtain. Comparatively, the deployment of image-based gauging techniques based on LSPIV [cf. *Muste et al.*, 2008] or STIV [*Fujita et al.*, 2007] methods is more difficult and, until recently, their application to hydrometry has been restricted to specialized research teams [cf. e.g., *Dramais et al.*, 2011]. The use of a Fluvial Acoustic Tomography [*Kawanisi et al.*, 2012] is likewise restricted to research teams.

A variety of nonportable Doppler radars for surface velocity measurement have been developed since the early 2000s especially in the USA and Japan. Tested setups include fixed instruments installed under bridges [*Fukami et al.*, 2008; *Lee and Julien*, 2006; *Yorozuya et al.*, 2010], deployed using cableways [*Plant et al.*, 2005], fixed or van-mounted radars deployed on banks [*Cheng et al.*, 2004; *Costa et al.*, 2000, 2006; *Lee et al.*, 2002; *Teague et al.*, 2001] as well as aircraft-mounted devices [*Melcher et al.*, 2002; *Plant et al.*, 2005]. The majority of target water bodies are large rivers with average widths in the range of 100–1000 m. In many cases, instrumentation was set up for continuous acquisition of velocity data under unsteady flow conditions, and simultaneous contact measurements were carried out to validate velocity measurements and discharge estimates. Overall, discharges measured using nonportable, noncontact devices range between 100 and

4500 m³/s. Despite their potential, the widespread use of these radar devices is limited by the need for fixed structures or machinery and by their cost, which has been in the order of \$10,000 in the last decade.

In contrast, handheld radars represent a cheaper, easy-to-use solution to gauge multiple field sites, even at short notice. However, the uncertainty of such new velocimetry techniques requires assessment and information on the optimal use and performance is still limited. Most importantly, a surface to depth-averaged velocity ratio (referred to as the velocity coefficient, α) must be quantified to compute discharge from non-contact data. Theoretical formulations and experimental evidence have been used to set this parameter [Le Coz *et al.*, 2010], but information on its dependence on flow conditions is sparse. Moreover, it is crucial to identify potential sources of error, such as changes in the cross-sectional topography that can occur between the velocity measurements and the bathymetry surveys when undertaken asynchronously.

In the present study we report on a large set of tests of application of the Surface Velocity Radar for velocity gauging in a wide range of riverine contexts. To the authors' knowledge, only few field-scale tests of handheld radar velocimeters have been published [Tamari *et al.*, 2013, 2014], but no attempt has been made to systematically evaluate the uncertainty of SVR-based discharge estimates. Discharge was often derived from a single surface velocity measurement [Corato *et al.*, 2011; Fulton and Ostrowski, 2008] using a probability distribution function [Chen and Chiu, 2004]. In gauged rivers including both small creeks (discharge ~ 10 m³/s) and larger rivers (300–900 m³/s) the errors in discharge estimation range between 2 and 8%. Tamari *et al.* [2014] used an SVR to reconstruct the transverse distribution of surface velocity at laboratory and field scale, but no discharge estimation was derived from these gaugings. In addition, the present study provides examples of SVR use in small channels, where high roughness conditions can affect the accuracy of discharge values computed with velocity-area methods.

This study presents a systematic testing of a portable Surface Velocity Radar with the following specific goals: i) to assess the variability of the velocity coefficient within a broad range of morphological and hydraulic conditions (depth, width, relative roughness); ii) to evaluate the accuracy and repeatability of velocity and discharge estimates; and iii) to identify optimal instrument deployment and effective operational choices.

2. Methods

2.1. Principles of Radar Velocimetry

Noncontact radar velocimeters make use of the Doppler effect to provide an estimate of water surface velocity. Radar units emit a radio signal that is backscattered to the antenna by short surface waves generated by turbulence, rain or wind [Costa *et al.*, 2006; Plant *et al.*, 2005]. The length of the scattering waves λ_b is given by the Bragg condition as

$$\lambda_b = \frac{\lambda}{2\sin\theta}, \quad (1)$$

where λ is the wavelength of the incident beam and θ is the incidence angle (tilt).

Scatterers move with respect to a fixed antenna because of their intrinsic speed (phase speed) and because of advection by the underlying river current, producing a difference in frequency between the transmitted and the return signals (Doppler shift). Signal processing allows derivation of the component of the scatterer's velocity in the direction of the antenna. Surface flow velocity is computed by taking into account the vertical (tilt) and horizontal (yaw) angles of the beam.

The return signal represents an average over the beam footprint on the river water surface, also referred to as illuminated area. The beam footprint is an ellipse, the area of which depends on the horizontal beam width and the distance between the antenna and the target. As a consequence, velocity values are averaged over increasingly large areas as the distance between the instrument and the water surface increases. This is a weighted average velocity according to the angular pattern of the radar beam's energy. Limited theoretical knowledge of this weighted average is available to users [Decatur Electronics, 2011].

Radar-based velocity results are unreliable when the return signal strength is too weak, typically when the free surface of the water is too smooth. In this case, specular reflection of the radar beam dominates over Bragg scattering. Return signal strength increases for larger tilt angles, but so do velocity projection errors.

A trade-off value should therefore be found in the allowable tilt range (typically $<60^\circ$). Finally, radar velocities are also affected by fixed targets, rain and wind shear at the free surface [Costa *et al.*, 2006].

2.2. Radar Deployment

In the present study we tested two equivalent versions (so-called V1 and V2 by the manufacturer) of the handheld Decatur Surface Velocity Radar (SVR), also used by Fulton and Ostrowski [2008] and Corato *et al.* [2011]. The SVR has a horizontal beam width of 12° , a claimed measurement accuracy equal to 5% of reading and a measuring range of 0.1–9.1 m/s. For each measurement, the instrument returns ten subsequent velocity values averaged over five seconds and a global average velocity [Decatur Electronics, 2011]. The unit is equipped with a tilt sensor for automatic internal compensation of the tilt angle (up to 60°), while the horizontal angle (yaw) with respect to the flow direction requires manual assignment. The SVR uses a K-band, IACP type III antenna with a nominal transmission frequency of 24.15 GHz, corresponding to a wavelength of approximately 1.2 cm. As a consequence of the Bragg condition, waves of a few millimeters in length need to be present on the water surface. Although no complete calibration was performed [Jendzurski and Paulter, 2009], transmission frequency was verified using a tuning fork.

Velocity was sampled along target cross sections either by wading (“in-stream” deployment) or by taking measurements from river banks, from bridges, or from other structures spanning the river. Examples of deployment methods are depicted in Figures 1a–1d, while Figures 1e and 1f provide schemes of the main geometry parameters. Tilt angle θ was chosen on the basis of horizontal and vertical distance (d_h and d_v , respectively) between the target cross section and the antenna and set using a tripod. Beam footprint width along the cross section (R) was calculated from the oblique distance (d_o) between the SVR and the water surface; the transverse spacing of measurements was chosen accordingly to ensure complete coverage of the target cross section. Surveying points were marked on the ground to facilitate the repetition of measurements over time.

2.3. Complementary Measurements

Simultaneous velocity measurements were carried out using conventional contact techniques (current meters, ADCPs), but also nonportable radars, floats and Large Scale Particle Image Velocimetry (LSPIV). Simultaneous surveys provided benchmarks for the evaluation of the accuracy of radar-derived discharge data (in analogy with previous studies; see Costa *et al.* [2006]; Fukami *et al.* [2008]; Fulton and Ostrowski [2008]; Lee and Julien [2006]; Lee *et al.* [2002]; Plant *et al.* [2005]; Tamari *et al.* [2014]; Teague *et al.* [2001]; Yorozuya *et al.* [2010]).

Complementary measurements were generally deployed according to usual best practice guidelines (ISO748 for current meters and floats and USGS/ISO guidance for ADCPs). Gauging with flow meters was performed using wading rods in small mountain streams (width 10–20 m, typical depth 20–70 cm). Instrumentation includes mechanical (Ott C31, SEBA M1) and electromagnetic sensors (Flo-Mate, Marsh-McBirney model 2000, SEBA FlowSens). For larger rivers, (width 100 m, at typical depth) current meters and ADCP sensors were deployed from cableways or bridges following routine procedures defined by operational hydrological services. ADCP models include Sontek M9 and Teledyne RD RioGrande, StreamPro and RiverRay. Data from a fixed Ott Kalesto Radar installed under a bridge were also used. A comparative analysis of data obtained using a broad range of techniques and instruments allowed to minimize the possible systematic errors associated with a specific instrument, technique or site.

Water stage records and official rating curves were provided by local water management agencies. Cross-sectional geometry was reconstructed by combining water depth profiles obtained from current meter/ADCP surveys and topographical surveys of bank areas.

2.4. Computation of Discharge

2.4.1. Velocity-Area Methods

Discharge was computed using the midsection velocity-area method [cf. e.g., Le Coz *et al.*, 2012]. Following this method, total cross-sectional area is divided into vertical subsections, or panels, centered on velocity survey positions. Panel area A_i associated with the i -th velocity value extends to half-distance from neighboring verticals in both directions (see Figure 1e) and is computed as

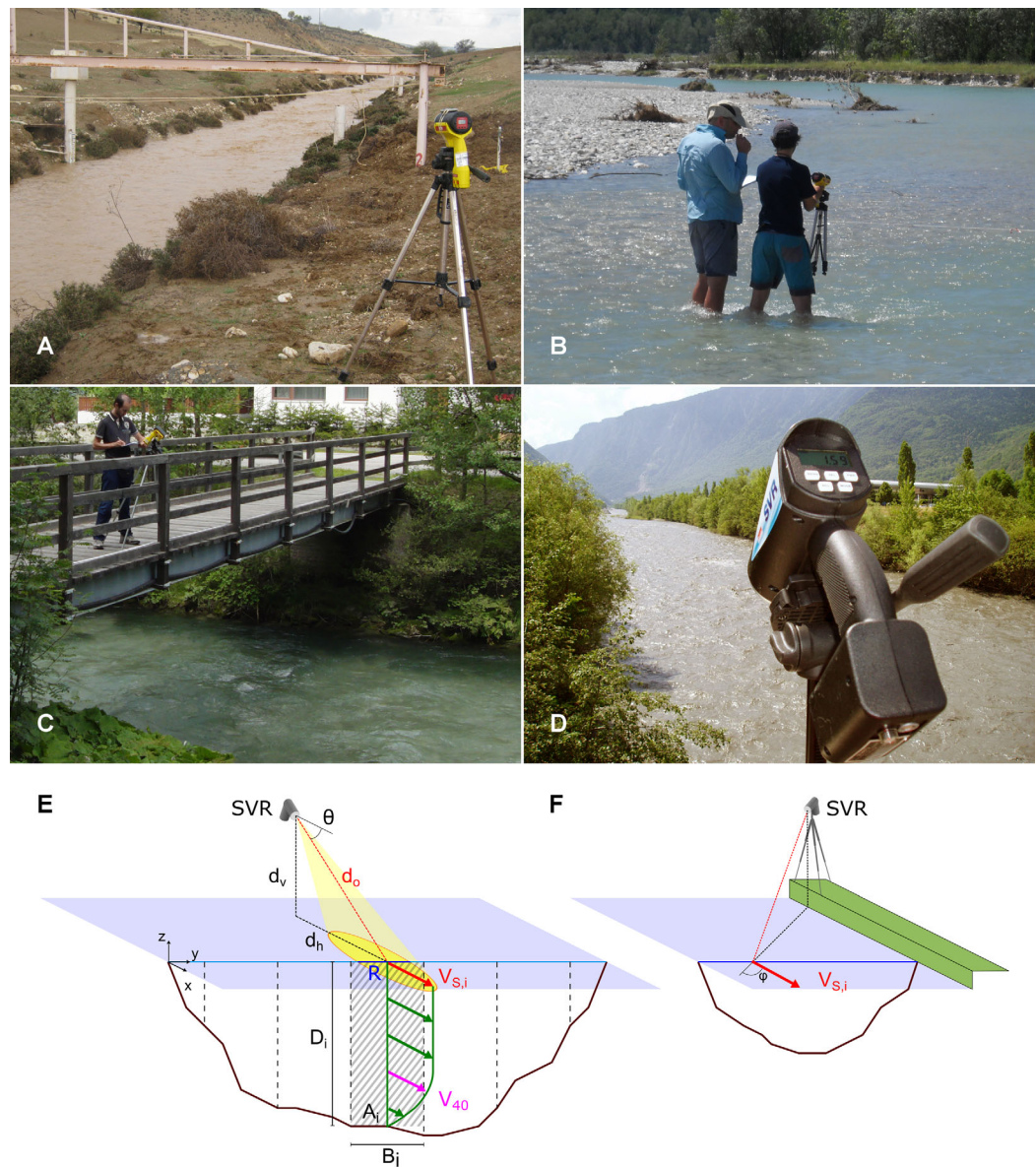


Figure 1. Schemes of SVR operation. (a) deployment from bank in Wadi Eshtemoa, Israel; (b) in-stream deployment in the Tagliamento River, Italy; (c) deployment from a low bridge in the Rienza River, Italy; (d) measurements at high flow from a bridge in the Arc-en-Maurienne River, France; (e, f) main geometry parameters for SVR surveys: B_i , D_i and A_i represent width, local depth and area of the i -th panel, $V_{s,i}$ is local surface velocity, θ is tilt angle and d_v , d_h , and d_o are the distances between the antenna and the water surface in the vertical and horizontal direction and along the radar beam, respectively. R is the beam footprint size along the cross-section. In (F), ϕ is the yaw angle.

$$A_i = B_i D_i, \tag{2}$$

where B_i is panel width and D_i is local depth. In the case of simultaneous contact/noncontact measurements, the same channel cross-sectional geometry data set was used to compute discharge from surface velocity values, as SVR surveys have no associated depth data. This choice implies that i) total cross-sectional area is identical for simultaneous measurements and ii) in the case of SVR data, geometry is usually sampled over a denser set of points compared to velocities. For all surveys, edge areas (extending between the banks and the first/last vertical) were assigned a local velocity value equal to that of the closest vertical. Both bed geometry and water stage were assumed to be constant during each SVR survey. Moreover, because of the difficulty of obtaining bed elevation profiles during floods, we used geometry data acquired before or after the event. While these simplifying assumptions are widely used, they represent a source of uncertainty for discharge estimation.

Total discharge Q was computed as the sum of discharge contributions of each panel Q_i

$$Q_i = A_i V_i, \tag{3}$$

where V_i is the depth-averaged velocity in the i -th subsection. In the case of conventional contact measurements, V_i was computed from velocity values measured at given depths in accordance with ISO 748 guidelines.

2.4.2. Computation of Discharge From SVR Data

The velocity-area method was similarly applied to surface velocity data acquired with SVR. An alternative procedure requiring a single surface velocity measurement along the cross section [Chen and Chiu, 2004; Chiu et al., 2005] has been applied, for example by Fulton and Ostrowski [2008] and Corato et al. [2011]. This method is based on the regularity of transverse and vertical velocity distributions and in particular on the assumption that the location of the maximum velocity along the cross section is stable over time and independent of flow stage. As this hypothesis is not supported by field data at some of the field sites surveyed for the present study, this procedure was not applied.

Discharge computation from SVR data requires the calculation of depth-averaged velocity V_i from measured surface velocity $V_{s,i}$. This is accomplished by defining a velocity coefficient α

$$\alpha = \frac{V_i}{V_{s,i}}. \tag{4}$$

The choice of α is a key issue in any noncontact gauging technique and therefore a variety of approaches were tested and compared in the present study, namely i) "default" α derived from the literature; ii) "calibrated" α obtained exclusively from contact velocity profiles; iii) "local" and "global" α derived from simultaneous contact and SVR measurements and iv) "theoretical" α derived from classical open-channel flow formulations.

Default α was set to 0.85, a widely accepted value employed in many riverine contexts [see Fukami et al., 2008; Le Coz et al., 2010, 2012; Muste et al., 2008; Rantz, 1982; Yorozuya et al., 2010]. Calibrated α was obtained by fitting a power or logarithmic law to individual vertical velocity profiles obtained with current meters or ADCP. Velocity usually increased monotonically with depth and no marked dip phenomenon was observed [Lassabatere et al., 2012; Wang et al., 2001]. Surface velocity was thus computed by extrapolating the profiles to the surface. At each site, calibrated α values were averaged along the cross section.

Local α values were computed as the ratio between depth-averaged velocities obtained with conventional contact techniques and simultaneous SVR data. Subsequently, a global value of α was computed at each cross-section as the ratio between discharge estimates derived from depth-averaged velocity profiles (Q_{ave}) and from surface velocity profiles (Q_s). This is equivalent to a weighted average of local α values, where panel areas are used as weights.

2.4.3. Theoretical Formulation for the Velocity Coefficient

The vertical velocity distribution for open-channel turbulent flows in wide, uniform, smooth-bed channels is usually assumed to follow a logarithmic distribution extending over most of the water column [cf. e.g., Smart, 1999]. Local flow velocity variations along the vertical coordinate z can be written as follows:

$$u(z) = \frac{u^*}{k} \ln\left(\frac{z}{z_0}\right). \tag{5}$$

Here u^* denotes friction velocity, z_0 is the roughness length and k is the Von Kàrmàn constant ($k=0.41$). Assuming that (4) applies over the whole flow depth D_i , depth-averaged velocity V_i can be computed as

$$V_i = \frac{1}{D_i - z_0} \int_{z_0}^{D_i} u(z) dz = \frac{u^*}{k} \left[\ln\left(\frac{D_i}{z_0}\right) - 1 \right]. \tag{6}$$

Surface velocity V_s can also be derived from (5) by setting $z=D_i$. Therefore, it is possible to compute a theoretically-derived coefficient α that expresses the ratio between depth-averaged and surface velocity values for a purely logarithmic velocity profile extending from a reference height ($z=z_0$) up to the free surface ($z=D_i$):

$$\alpha = \frac{D_i}{D_i - z_0} - \left[\ln \left(\frac{D_i}{z_0} \right) \right]^{-1}. \quad (7)$$

When relative submergence of roughness elements is high, i.e., when $z_0 \ll D_i$, the expression of α reduces to

$$\alpha = \frac{L_0 - 1}{L_0}; \quad L_0 = \ln \left(\frac{D_i}{z_0} \right). \quad (8)$$

α is referred to as the “velocity coefficient” in the rest of the paper. Alternatively, the vertical velocity distribution can be expressed using a power law formulation [as reported in ISO 748], which leads to

$$\alpha = \frac{m}{m+1}, \quad (9)$$

where $1/m$ is the exponent of the power law [Le Coz et al., 2010]. This formulation coincides with the simplified solution for the logarithmic velocity profile for $m = L_0 - 1$.

In its theoretical formulation, α depends only on the dimensionless roughness length z_0/D_i and is therefore written as a function of relative roughness, i.e., the ratio between a representative roughness height d_s and flow depth D_i . The relationship between z_0/D_i and d_s/D_i is given by

$$\frac{z_0}{D_i} = e^{-kC_f - 1}, \quad (10)$$

where the friction factor C_f is expressed by means of the widely used formula of *Engelund and Hansen* [1967]:

$$C_f = \frac{V_j}{u^*} = 6 + 2.5 \ln \left(\frac{D_i}{2.5 d_s} \right). \quad (11)$$

The so-called “logarithmic layer,” i.e., the region where the vertical velocity profile can be correctly approximated by a logarithmic law, progressively reduces for increasing relative roughness, i.e., for flows with high relative submergence and for irregular rough beds [Dittrich and Koll, 1997; Nikora et al., 2001]. The logarithmic velocity profile has, indeed, been shown to be valid at large enough distances from the rough bed compared to the roughness height [Smart, 1999]. When roughness height approaches the flow depth (e.g., 0.2–0.5 D_i) the logarithmic layer almost disappears and the flow is considerably affected by skin friction and form drag associated with spatial heterogeneity related to the protruding roughness elements within most of its depth [Nikora et al., 2007].

Under such conditions, where the local, turbulence-averaged velocity values are extremely heterogeneous, the most suitable approach to describe flow properties has been shown to require a further averaging in the space domain, subsequent to the time-averaging that leads to the Reynolds-averaged Navier-Stokes equations [Nikora et al., 2001].

3. Study Sites

Field data were collected between 2010 and 2013 in Israel, Italy and France. Survey sites cover a wide range of channel sizes and types, velocity, discharge and channel roughness values. Moreover, all sites provide the opportunity to compare radar-based surveys with independent, simultaneous measurements of velocity and discharge acquired with alternative methods. Table 1 summarizes the key properties of target cross sections. Field sites can be grouped as follows: (a) shallow mountain streams (Casies, Noce, Drava and Rienza, Italy; Neste, Giffre, Eau d’Olle, Vence, Salat, Arc-en-Maurienne, Volane, France); (b) braided river anabranches (Tagliamento River, Italy); (c) semiarid/arid climate streams (Wadi Eshtemoa and Ein Fesh’ha, Israel); (d) large piedmont rivers, either channelized (Adige, Italy; Rhône and Isère, France) or with a more natural morphology (Ardèche and Ain, France); (e) small lowland rivers (Bienne, Palhère, Bourbre, Ratier and Charbonnières, France); (f) large lowland rivers (Garonne and Saône, France); and (g) artificial channels (outflow canal of the Mezzocorona hydropower plant, Italy). Examples of deployment of the SVR instrument in the field are shown in Figure 1.

Table 1. Synthesis of Hydraulic and Geometry Conditions for the Study Sites^a

Site Name	Water Course	Group	d_{50} (mm)	S (%)	W (m)	D_m (m)	d_{50}/D_m	Q_{SVR} (m ³ /s)	max V_s (m/s)	d_o (m)	θ (°)
Colle Casies	Casies (I)	a	250	0.62	7	0.46	0.547	3.1	1.41	3.6	40
Pellizzano	Noce (I)	a	100	0.40	19	0.35 to 0.41	0.247 to 0.285	5.6 to 8.4	1.10 to 1.56	11.5	30
Versciaco	Drava (I)	a	150	0.50	8	0.56	0.266	3.2	1.19	6.7	36
Monguelfo	Rienza (I)	a	175	0.44	9	0.69	0.363	8.1	1.66	10.8	24
Beyrède	Neste (F)	a	100	0.70	17	0.75	0.133	10.4	1.36	4.9	45
Taninges	Giffre (F)	a	80	0.50	33	0.60	0.133	22	1.96	11.0	45
La Pernière	Eau d'Olle (F)	a	50	0.40	11	0.40	0.125	2.5	1.08	7.8	45
Pont de Vence	Vence (F)	a	50	0.17	5.5	0.50	0.100	2.2	1.18	4.9	45
Pont du Giffre	Giffre (F)	a	80	0.50	16	1.00	0.080	28	2.85	8.1	45
Roquefort	Salat (F)	a	80	0.40	66	1.20	0.067	56	1.26	9.9	45
Saint-Arve	Arc-en-Maurienne (F)	a	80	0.50	35	1.50	0.053	23	4.70	11.3	45
Vals-les-Bains	Volane (F)	a	40	0.80	40	0.70 to 1.00	0.040 to 0.057	7.8 to 24	4.79	4.2	45
Braulins 1	Tagliamento (I)	b	30	0.19	6	0.23	0.133	0.9	1.11	5.1 to 48.9	13
Braulins 2	Tagliamento (I)	b	30	0.32	10	0.18	0.163	0.7	0.57	6.3 to 47.1	11 to 14
Braulins 3	Tagliamento (I)	b	37	0.38	10	0.51	0.072	7.5	1.83	58.1	11
Braulins 4	Tagliamento (I)	b	55	0.75	16	0.22	0.254	2.7	1.06	6.3 to 47.1	11 to 14
Cornino 1	Tagliamento (I)	b	28	0.30	22	0.30	0.095	5.7	1.28	5.1 to 15.4	13
Cornino 2	Tagliamento (I)	b	45	0.19	11	0.28	0.160	2.4	1.52	5.1 to 15.4	13
Venzone	Tagliamento (I)	b	58	0.28	67	0.59	0.099	55	2.17	40.1	3
Eshtemoa	Eshtemoa (ISR)	c	17	0.75	6	0.20 to 0.65	0.026 to 0.085	0.8 to 8.1	0.79 to 2.58	8.9	13
Ein Fesh'ha	Ein Fesh'ha (ISR)	c	3	2.30	1.2	0.28	0.011	0.1	0.70	7.1	18
Pont d'Ucel	Ardèche (F)	d	100	0.50	160	2.00	0.050	98	6.05	12.7	45
Bronzolo	Adige (I)	d	100	0.12	64	2.26 to 2.32	0.044	247 to 261	2.25 to 2.49	16.6	33 to 35
San Lorenzo	Adige (I)	d	30	0.10	70 to 90	0.98 to 4.30	0.007 to 0.031	70 to 1121	1.49 to 3.92	33.9 to 56.3	9 to 12
Surjoux	Rhône (F)	d	50	0.056	73.5	3.00	0.017	281	2.10	11.3	45
Chazey	Ain (F)	d	15	0.15	73	2.10	0.007	179	2.26	7.8	40
Grenoble Campus	Isère (F)	d	5	0.06	70	1.50 to 1.75	0.003	142 to 221	1.83 to 2.05	14.1	45
Saint-Claude	Bienne (F)	e	50	0.0054	20	1.00	0.050	34	2.31	11.3	45
La Palhère	Palhère (F)	e	20	0.05	2	0.60	0.033	0.8	0.99	4.4	45
Jameyzieu	Bourbre (F)	e	10	0.05	30	1.00	0.010	23	1.01	2.8	45
Saint-Genis-les-Ollières	Ratier (F)	e	1	0.10	2.9	0.40	0.003	1.0 to 1.5	0.70	2.8	45
Charbonnières-les-Bains	Charbonnières (F)	e	1	0.10	5.9	0.60	0.002	0.9	0.70	9.9	45
Mancioux	Garonne (F)	f	10	0.30	45	3.00	0.003	100	1.23	14.1	45
Lyon Saint-Georges	Saône (F)	f	20	0.03	100	8.50	0.002	1670	2.70	11.3	45
Lamagistère	Garonne (F)	f	2	0.08	170	5.80	0.0003	2270	3.11	17.0	45
Mezzocorona	Power plant outlet (I)	g	1	0.01	13	1.41	0.001	20	1.76	11.9	30

^aS and W are the local slope and channel width, respectively. Max V_s is the maximum value of the surface velocity measured with SVR and d_o is the distance between the target cross-section and the antenna along the radar beam. Relative roughness d_{50}/D_m is computed as the ratio between median grain size d_{50} and mean channel depth D_m . See section 3 for grouping criteria.

Flow regime is perennial at all sites except Wadi Eshtemoa, which is active about 7 days per year and is subject to flash floods that are often initiated as bores driven on a dry riverbed. In the Ain, Adige and Noce Rivers, flow regime is strongly affected by hydropeaking. All cross sections belong to gravel bed rivers, with the exception of Ein Fesh'ha, where the channel incises into cohesive, almost vertical banks, Bourbre and Ratier, which have sand beds, and Mezzocorona, which is a stone-lined trapezoidal canal.

Channel width ranges between 1 and 170 m and maximum observed flow depth ranges between approximately 0.3 and 5.5 m. Relative roughness, computed as the ratio between median grain size and mean channel depth, ranges between 0.0003 (Garonne at Lamagistère) and 0.6 (Casies creek). Repeat surveys were carried out on the Eshtemoa, Adige and Noce Rivers. In particular, 19 measurements were performed at the San Lorenzo station on the Adige River, covering a wide range of flow conditions (about 70–1100 m³/s). At each site, at least one set of concurrent radar and contact velocity measurements is available. Conventional velocity surveys were carried out by the Servizio Idrografico of the Regione Friuli Venezia Giulia (Venzone site), the Ufficio Dighe of the Autonomous Province of Trento (San Lorenzo site) and the Ufficio Idrografico of the Autonomous Province of Bolzano (Bronzolo, Versciaco, Monguelfo and Colle Casies sites). Official rating curves and water level data were also provided for the same sections, with the exception of Venzone. Discharge data for the Mezzocorona power plant were provided by Dolomiti Edison Energy.

For French sites, SVR and concurrent velocity measurements were achieved by hydrometry staff of Irstea, Electricité de France (EDF), Compagnie Nationale du Rhône (CNR) and the national hydrological services (DREAL Rhône-Alpes). Rating curves and water level data were also provided by the same organizations.

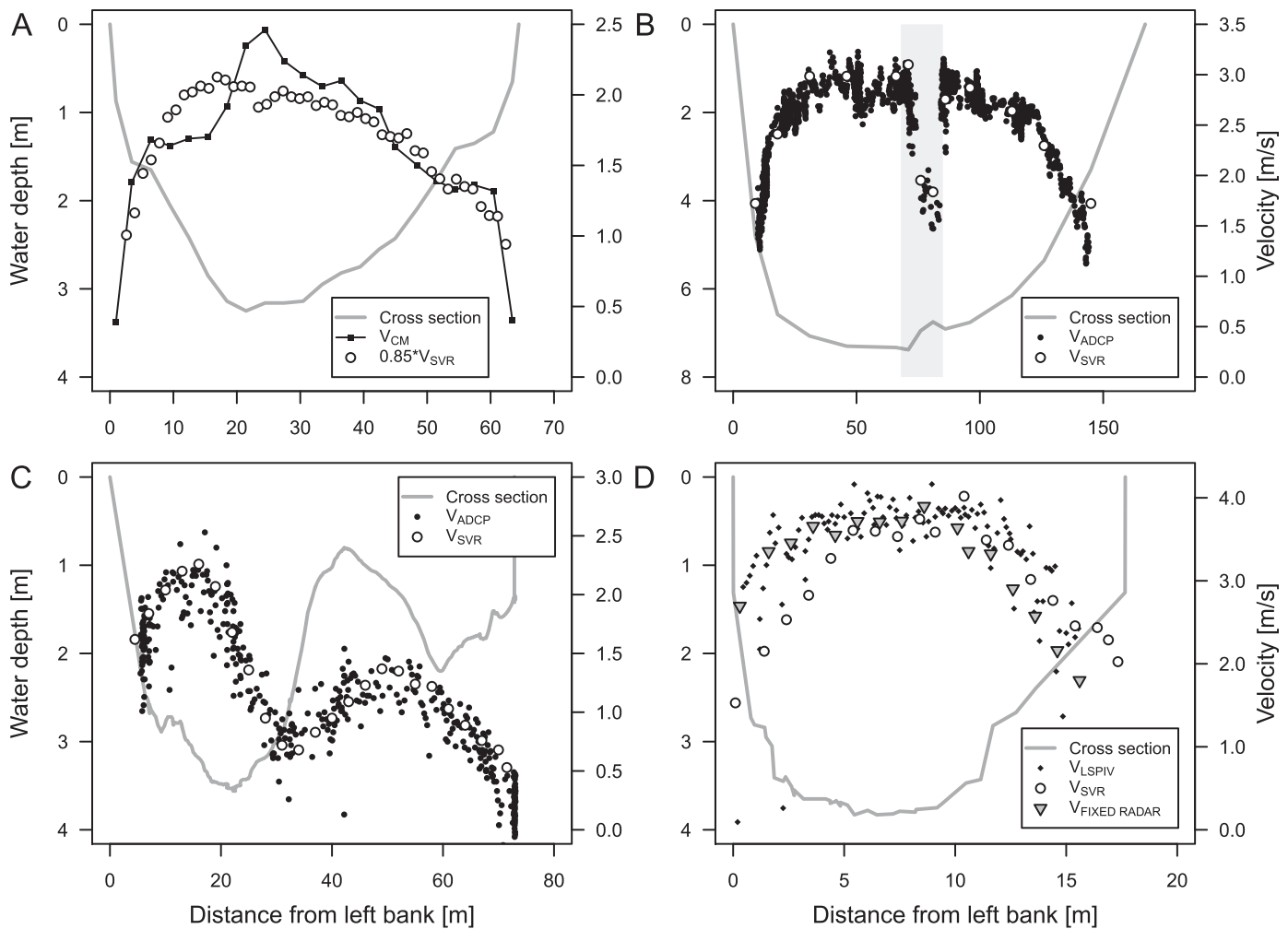


Figure 2. Comparison between SVR surveys and other velocity survey techniques. (a) SVR and depth-averaged velocity obtained with a mechanical current meter, Adige River at Bronzolo, Italy. SVR estimates were multiplied by the default value of the velocity coefficient (0.85); (b) SVR and ADCP topmost bins, Garonne at Lamagistère, France. The shaded area corresponds to the wake of a bridge pier; (c) SVR and ADCP topmost bins, Ain at Chazey, France; (d) SVR, fixed radar and LSPIV, Arc-en-Maurienne at Randens, France.

4. Results

4.1. Surface Velocity Data

4.1.1. Comparison With Other Surface Velocity Measurements

As a first step, transverse surface velocity profiles obtained with radar devices were compared with simultaneous surveys carried out with other stream gauging techniques. At most sites conventional methods such as current meters and ADCP were used as benchmarks because of their widespread use and well documented uncertainty. However, caution is required when directly comparing velocity data obtained with different methods as they represent spatial averages over different areas/volumes. For this reason, contact measurements were averaged over vertical panels corresponding to the width of the radar beam footprint (R , see Figure 1).

Contact measurements were carried out on the Adige River at Bronzolo using a mechanical current meter deployed from a cableway. Figure 2a provides a comparison between depth-averaged velocity values and SVR data multiplied by default α (0.85). Transverse velocity profiles are in fairly good agreement, but local differences as high as 20% can be observed. However, since the area under the two velocity profiles is similar and the cross section has a fairly regular geometry, discharge estimates obtained with the two methods are expected to be similar.

SVR-ADCP comparisons are shown for the Garonne River at Lamagistère (Figure 2b) and for the Ain River at Chazey (Figure 2c). ADCP surveys were performed using a Teledyne RDI RioGrande 1200 kHz and a RDI

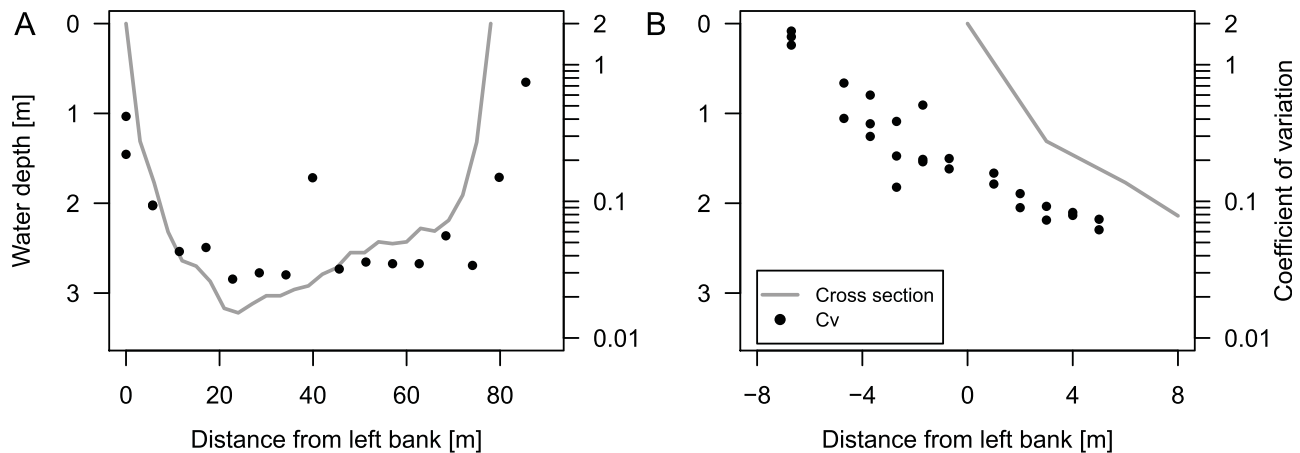


Figure 3. Repeatability of SVR data at the San Lorenzo site on the Adige River expressed as coefficient of variation. (a) Global cross-sectional distribution; (b) detailed set of c_v values for the left bank area. The transverse position of SVR velocity data corresponds to the position of the antenna.

RiverRay 600 kHz, respectively, and velocities recorded in the topmost bins were used as benchmarks. At these sites, both SVR and ADCP surveys captured the transverse variability of velocity caused by local obstacles and properties of cross-sectional geometry (the wake of a bridge pier in the Garonne and a central bar in the Ain). SVR velocities are within 5% of ADCP data for most of the Garonne cross section but increase to 15% close to the banks and in the wake of the pier. On the Ain, ADCP data show larger spatial fluctuations and differences with SVR readings are typically within 15%.

Radar-derived velocity values were directly compared with other surface velocity survey techniques. LSPIV and fixed radars were used on the Arc-en-Maurienne River at Randens (see Figure 2d). SVR errors with respect to either technique do not exceed 10% in the central part of the cross section. Finally, floats were used on the 6 m wide Wadi Eshtemoa. Here local error is as high as 25% at low flow, but decreases to less than 7% at higher flows.

In most cases, discrepancies are larger near the banks, possibly because SVR deployment from bridges produces large illuminated areas that include both fast-flowing zones and near-bank recirculation areas with low velocities. Large averaging areas also tend to produce flatter transverse distributions, as shown for the SVR survey on the Adige River at Bronzolo (Figure 2a, radar beam footprint width R 3.3 m). The influence of near-bank areas is expected to be larger in small channels like Wadi Eshtemoa, where radar-based measurements were acquired from a single point with the illuminated area covering the entire channel width.

In general, SVR estimates of transverse velocity profiles are in good agreement with contact measurements despite local over- or underestimation, showing that radar-based instruments are a valid option for obtaining reliable, noncontact surface velocity data when specific, local details are not of interest.

4.1.2. Repeatability of Velocity Measurements

The occurrence of spurious velocity values was observed during measurements especially close to the banks, where local recirculation, currents and eddies are associated with the near-bank boundary layer and sometimes also with partially submerged vegetation. To evaluate the repeatability of radar-based velocity data, multiple measurements were taken at the same location under steady flow conditions and the coefficient of variation (c_v , the ratio of the standard deviation to the mean), was computed for raw instrument outputs (sets of ten consecutive readings acquired with a 5 s interval).

In the large, channelized Adige River (Bronzolo and San Lorenzo sites), c_v fluctuates between 0.02 and 0.07 in the central part of the cross sections while much higher values (up to and sometimes exceeding 0.30) are observed for areas close to the bank, as shown in Figure 3a. Figure 3b includes a set of additional measurements with a transverse spacing of 1 m covering the left bank region. In this case, the antenna was moved to the left until the illuminated area (R 11.4 m) was completely outside of the wetted cross section. This data set shows that the variability of velocity values increases as a larger part of the sampling area falls on a dry bank.

Shallow mountain creeks (Rienza, Casies, Noce) exhibit a fairly similar spatial trend of c_v , and, more importantly, similar overall values. Therefore, the repeatability of SVR measurements appears to be strongly linked with its position along the cross section, but independent of channel size and relative roughness.

These results suggest that the overall mean velocity value internally computed by the instrument can be influenced by spurious velocity readings. As noted in the Decatur SVR User's manual [Decatur Electronics, 2011], measurements showing large temporal fluctuations should be discarded and repeated. A better estimation of the actual surface velocity value can be obtained from simple statistical analysis of raw measurements. In the present study, surface velocity was evaluated as the median of the 10 values set whenever the entire record of raw values was available. However, considerable discrepancies between internal mean and median occur only for cross-section edge areas where both velocity and flow depth are small. As a consequence, discharge estimation is not expected to be strongly influenced by uncertainty in velocity values close to the bank.

4.1.3. Local and Global Velocity Coefficients

The availability of concurrent radar and contact velocity profiles provided the opportunity to estimate α from field data. Surveys were directly compared at each vertical, with the aim of exploring the spatial variability of the velocity coefficient at the panel scale. Local α values were computed for each current-meter/ADCP vertical by dividing the depth-averaged velocity by the surface velocity value corresponding to the closest position of the SVR antenna. This choice is based on the assumption that the reflected signal is stronger near the center of the beam footprint, as reported by the manufacturer (Decatur Electronics, personal communication, 2014). As noted before, care must be taken in pairing depth-averaged and surface velocity data because of different spatial domains used by the instruments for averaging. However, since transverse surface velocity profiles obtained with SVR are relatively smooth (see Figure 2), α values obtained for the same vertical with adjacent SVR values are expected to be similar.

The variation of local α values with relative roughness and with local water depth is shown in Figures 4a and 4b, respectively. In this case, relative roughness is computed as the ratio between median grain size d_{50} (assumed constant over the cross section) and local channel depth D_r . Overall, local α values show substantial scatter (interquartile range 0.73–0.99, 1st–9th decile interval 0.51–1.12). Variability is large in shallow channels and drops rapidly for relative roughness values smaller than approximately 0.02–0.04. In large, deep rivers such as the Adige and the Ain, α fluctuates around the default value (0.85). An interesting case is represented by the Ein Fesh'ha, where velocity coefficient values are fairly stable despite the small size of the channel because of the low relative roughness with respect to other streams of comparable depth. The local variability of α shows no clear link with the distance between the antenna and the water surface. Stable α values have been obtained over a wide range of distances (from 10 m for the Ein Fesh'ha up to more than 50 m for the Adige River at S. Lorenzo). Therefore, the influence of the air gap is small in comparison with the effect of channel roughness.

Global values of the velocity coefficient were obtained as a weighted spatial average of local α . Figure 4c shows the variation of global α with the cross-section averaged relative roughness, computed as d_{50}/D_m . Overall, global α values are less scattered than their local counterparts (interquartile range 0.77–0.91, 1st–9th decile range 0.71–0.95). The default value of the velocity coefficient (dashed line) appears to be a fair approximation of global α for relative roughness values smaller than approximately 0.07, while larger dispersion occurs for rougher channels, where the vertical velocity distribution is not expected to follow a logarithmic profile.

Figure 4c also shows the theoretical velocity coefficient (solid line) obtained with formulations (7) to (11). For smooth channels, global α values are in good agreement with the theoretical solution. This is particularly true for the very smooth Lamagistère site on the Garonne River, where both global and theoretical α are larger than the default value. In rougher channels, the velocity coefficient tends to be more scattered and does not follow the decreasing trend obtained from analytical formulas.

The uncertainty of local and global velocity coefficients was computed as the standard deviation of α values, in accordance with ISO 748. The uncertainty of local and global α is equal to 0.25 and 0.13, respectively, corresponding to 29% and 15% of the default α value. The analysis was also applied separately to smooth (relative roughness ≤ 0.05) and rough (relative roughness > 0.05) channels. In the former case, the standard deviation of local and global α is equal to 0.12 and 0.06, respectively (14% and 7% of default α). Uncertainty

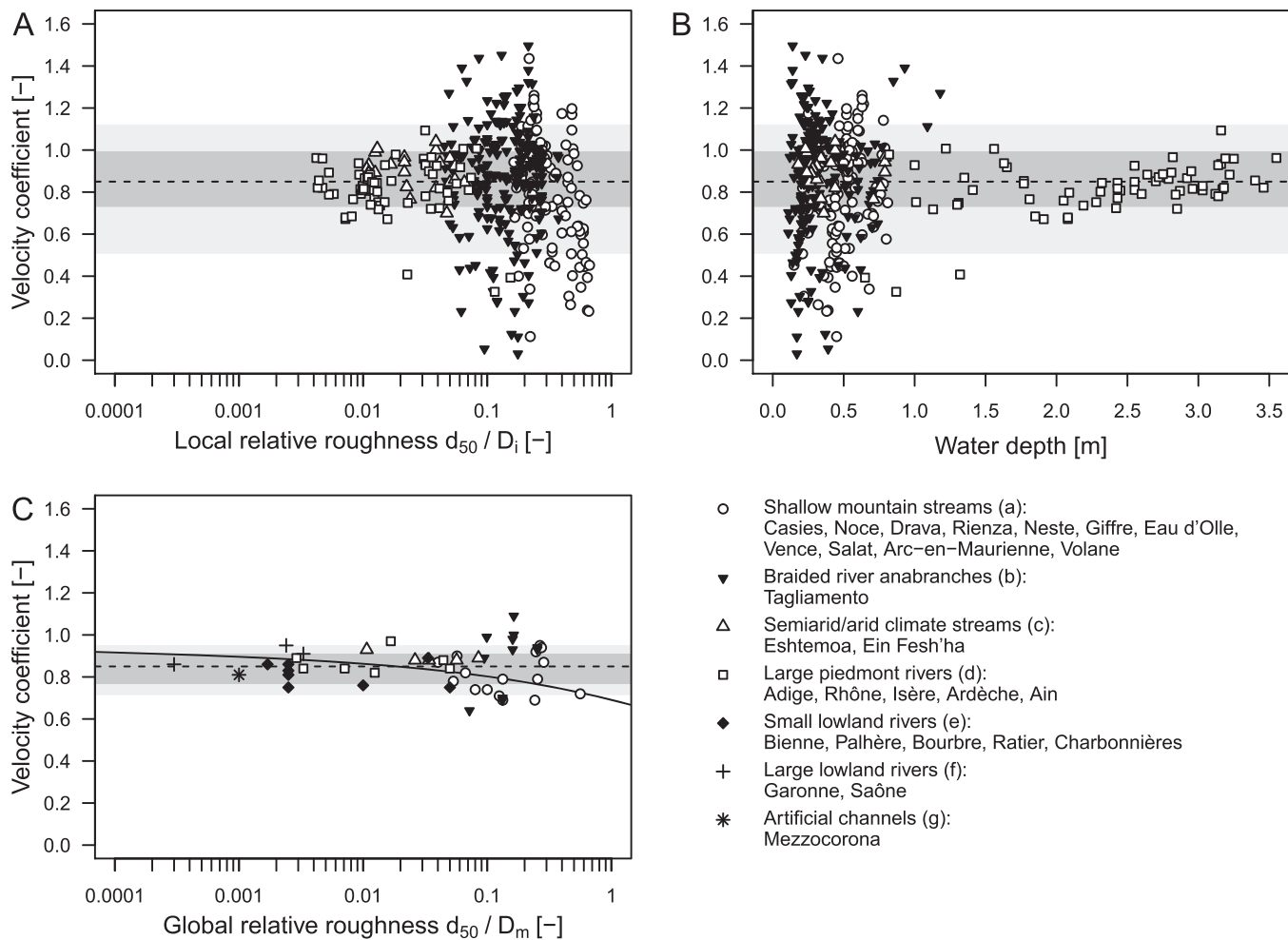


Figure 4. Variation of the local velocity coefficient with relative roughness (a) and local water depth (B) and variation of the global velocity coefficient with relative roughness (C). The dashed line represents the default value of the velocity coefficient (0.85). The solid line represents the theoretical velocity coefficient computed from equations (7) to (11). The interquartile range is shaded in dark grey; the 10th–90th percentile range is shaded in light gray. Local values of alpha are unavailable for some sites.

increases in rough channels (0.26 and 0.12 for local and global α , respectively, corresponding to 31% and 14% of default α).

4.2. Discharge Estimation From SVR Data
4.2.1. Comparison With Conventional Methods

Discharge was computed from SVR velocity surveys using (i) the default value of α ; (ii) a calibrated value derived from local velocity profiles as explained in section 2.3.2; (iii) the theoretical value of α as derived from equations (4)–(11). The SVR error was evaluated by comparing radar-based estimates with simultaneous contact surveys (if available) or with discharge values obtained from official rating curves. Complete results are summarized in Table 2; Figure 5 shows only error values computed with respect to simultaneous contact surveys.

In general, both default α (Figure 5a) and theoretical α provide discharge values within 10% of contact survey estimates if relative roughness is smaller than approximately 0.05. For calibrated α the same range of accuracy extends up to relative roughness values equal to approximately 0.1. Overall, 50% of the measurements presented here are within $\pm 8\%$ of corresponding contact surveys for default α and within $\pm 4\%$ for calibrated α . Interquartile ranges of error for low (≤ 0.05) and high (> 0.05) relative roughness correspond to -7 to 16% and -6 to 2% , respectively, in the case of default α , showing that better accuracy is to be expected for small to moderate relative submergence. In contrast, no considerable differences are observed in the case of calibrated α .

Table 2. Summary of Errors of Discharge Estimates Obtained With SVR^a

Site Name	Water Course	Gauging Method	Calibrated α	Theoretical α	Error, Default α (%)	Error, cal. α (%)	Error, Theor. α (%)
Colle Casies	Casies (I)	ADCP	0.79	0.73	12.1 to 18.4	4.2 to 10.1	-4.1 to -1.1
Pellizzano	Noce (I)	CM		0.76 to 0.77	-0.3 to 25.3		-12.8 to -13.1
Versciaco	Drava (I)	ADCP	0.82	0.76	-9.5 to -8.7	-12.7 to -11.9	-18.0 to -18.9
Monguelfo	Rienza (I)	ADCP	0.83	0.77	8.5	6.0	-2.3
Beyrède	Neste (F)	ADCP	0.71	0.79	23.3	3.0	14.9
Taninges	Giffre (F)	ADCP	0.77	0.79	7.4	-2.7	0.1
La Pernière	Eau d'Olle (F)	CM	0.72	0.79	20.0	1.6	12.2
Pont de Vence	Vence (F)	CM	0.77	0.80	14.5	3.7	8.1
Pont du Giffre	Giffre (F)	ADCP	0.80	0.81	14.9	8.1	9.5
Roquefort	Salat (F)	ADCP	0.80	0.82	3.1	-2.9	-1.0
Saint-Arve	Arc-en-Maurienne (F)	CM/RC	0.76	0.82	1.7	-9.0	-1.5
Vals-les-Bains	Volane (F)	RC		0.82 to 0.83	-6.0 to -2.4		-4.5 to -9.2
Braulins 1	Tagliamento (I)	CM		0.79	24.0 to 26.0		-17.4 to -15.3
Braulins 2	Tagliamento (I)	CM		0.78	-20.4 to -14.2		-26.5 to -20.8
Braulins 3	Tagliamento (I)	CM		0.81	31.5		26.0
Braulins 4	Tagliamento (I)	CM		0.77	-8.1 to -7.1		-17.2 to -16.3
Cornino 1	Tagliamento (I)	CM		0.80	-3.4		-8.6
Cornino 2	Tagliamento (I)	CM		0.79	-10.6 to -6.2		-17.5 to -13.3
Venzone	Tagliamento (I)	CM		0.80	-8.8		-13.8
Eshtemoa	Eshtemoa (ISR)	CM	0.88	0.81 to 0.84	-4.1 to -3.0	-0.2 to -0.7	-8.8 to -3.9
Ein Fesh'ha	Ein Fesh'ha (ISR)	CM		0.86	-8.3		-7.1
Pont d'Ucel	Ardèche (F)	RC		0.82	0.7		-2.3
Bronzolo	Adige (I)	CM/RC		0.83	-8.1 to -2.7		-10.4 to -5.1
San Lorenzo	Adige (I)	ADCP/RC		0.84 to 0.87	-12.4 to 6.6		-10.4 to 6.9
Surjoux	Rhône (F)	ADCP		0.85	-12.3		-12.0
Chazey	Ain (F)	ADCP	0.90	0.87	1.2	7.2	3.5
Grenoble Campus	Isère (F)	ADCP	0.88	0.88	-4.7 to 0.9	-1.3 to 4.4	-1.0 to 4.5
Saint-Claude	Bienne (F)	ADCP	0.81	0.82	13.0	7.7	9.6
La Palhère	Palhère (F)	CM	0.85	0.84	-4.9	-4.9	-6.4
Jameyzieu	Bourbre (F)	RC		0.86	12.1		13.8
Saint-Genis-les-Ollières	Ratier (F)	ADV/RC		0.88	-1.2 to 12.7		-2.9 to 17.3
Charbonnières-les-Bains	Charbonnières (F)	ADV		0.89	-0.7		4.0
Mancioux	Garonne (F)	ADCP	0.82	0.88	-0.8	-4.3	2.8
Lyon Saint-Georges	Saône (F)	ADCP	0.90	0.89	-10.4	-5.1	-6.6
Lamagistère	Garonne (F)	ADCP	0.92	0.91	-6.8	0.9	-0.6
Mezzocorona	Power plant outlet (I)	PT		0.90	4.8		10.4

^aReference discharge values were obtained with current meters (CM), pressure transducers (PT), ADV and ADCP or from rating curves (RC) if no contact measurements were available.

The use of calibrated α (Figure 5b) for smooth channels does not produce a substantial improvement of discharge estimates, with the exception of the Lamagistère site on the Garonne River and the Saône River at Lyon Saint-Georges. In both cases, measurements were taken during large floods, resulting in very low

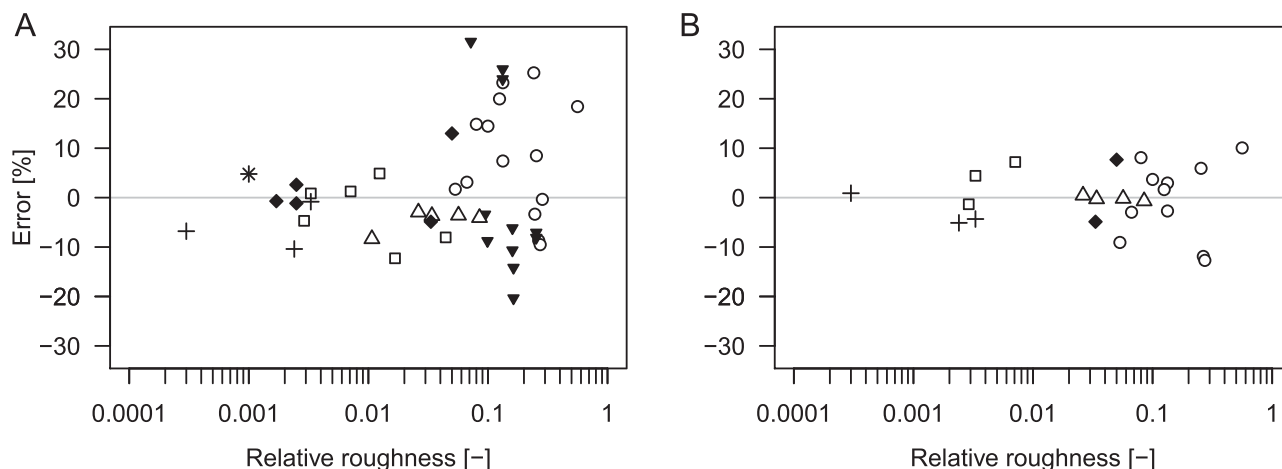


Figure 5. Differences between discharge estimates obtained with SVR and conventional methods using (A) default α and (B) calibrated α . Symbols are identical to those in Figure 4.

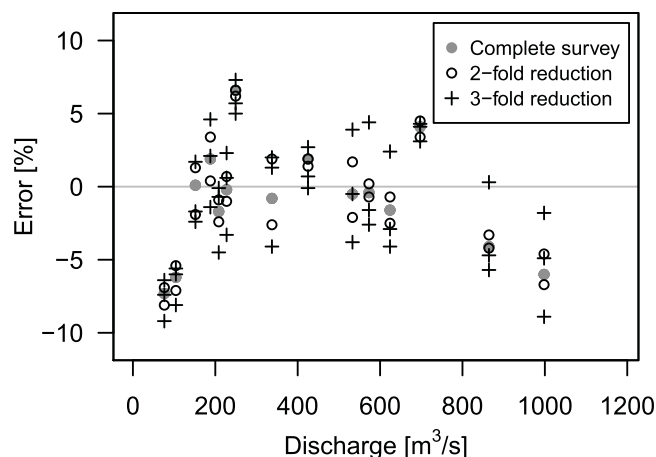


Figure 6. Error (as defined in equation 12) in SVR-derived discharge estimates with respect to rating curve values at the San Lorenzo gauging station (Adige River, Italy) for different spacings of transverse measurements: 5.7 m (complete survey); 11.4 m (twofold reduction); 17.1 m (threefold reduction).

relative roughness (< 0.001 and 0.002 , respectively). For the Garonne site, the SVR error obtained with default α is -7% but only 1% for calibrated α ($= 0.92$). Similarly, the error drops from 10.5% to 5% for the Saône River using calibrated α ($= 0.90$). In both cases, theoretical α values are very close to calibrated values and therefore the accuracy of resulting discharge estimates is also comparable. These results show that the use of default α can lead to an underestimation of discharge in very smooth channels, while both default and theoretical α are a good approximation for relative roughness in the range 0.002 – 0.05 . Within this range, theoretical α varies between 0.82 and 0.89 and discharges are within 4% of values computed with default α .

In rough channels (relative roughness > 0.05), the use of default α is expected to cause an overestimation of discharge as theoretical values of α are lower than 0.85 . This occurred for several SVR surveys (Braulins 1, Rienza, Casies, Arc-en-Maurienne, Bienne, Eau d’Olle, Vence, Giffre, Neste, Salat), with errors as high as 30% . However, discharge underestimation also occurred, even if negative errors are generally smaller. The use of calibrated α values yields much better results, for example for the Eau d’Olle and Neste sites where the SVR error drops from $\sim 20\%$ to 2 – 3% after calibration. In approximately one half of the cases, the use of theoretical α values represents an improvement with respect to default α , although errors close to 10% remain common.

The largest error was recorded at the Braulins 3 cross section, a moderately rough channel (0.072). Here SVR measurements were taken from a high bridge and the beam footprint width was comparable to channel width. Interestingly, the same configuration was used for Ein Fesh’ha, a much smoother channel, resulting in far better estimates of discharge. Thus, a single SVR measurement covering the entire cross section can be a reasonable operating choice in a smooth flow, while it may fail to capture the transverse variability of velocity in a rough flow.

In general, the error appears to be more strongly related to relative roughness than to other parameters. Errors around 10% were obtained for both small mountain streams (Drava, Rienza) and larger cross sections (Venzone, Tagliamento River), where average depth is similar but discharge and cross-section width are almost one order of magnitude larger.

Other cross-section properties may affect the relationship between SVR-derived discharge and reference contact gauging data. For example, mixed results were obtained for the Noce River, which is similar in size and relative roughness to the shallow Drava and Rienza Rivers. At the Pellizzano station, the error was lower than 3% in two cases and as high as 25% in one case. This cross section is located in a channelized reach with large cobbles (~ 200 mm in diameter) randomly placed on the river bed. Localized wake effects caused by these roughness elements may have affected contact measurements carried out with mechanical current meters.

Finally, on the Adige River at San Lorenzo, comparison with official rating curve data shows deviations ranging between -12% and $+7\%$ (see also Figure 6), with higher values both at low flow (< 250 m^3/s) and high flow (> 700 m^3/s). However, the rating curve is based on a set of conventional velocity surveys extending up to about 500 m^3/s and therefore care must be taken in using it to derive reference discharge values at higher flows.

4.2.2. Influence of Field Procedures: Effect of Number of Cross-Sectional Locations

At the San Lorenzo site on the Adige River, SVR velocity data were acquired at the same set of cross-sectional positions along the bridge for a wide range of flow conditions (70 – 920 m^3/s). The chosen

transverse spacing (5.7 m) resulted in considerable overlap (30–40%) of the illuminated areas. As a first step, discharge was computed using all surveyed velocity data. Afterward, we simulated a two or three fold increase in spacing of transverse measurements along the bridge by using velocity values acquired at i) every second transverse location; and ii) one in three transverse locations. All calculations were performed assuming $\alpha = 0.85$. The resulting discharge estimations (Q_n , with n multiple of the original spacing) were compared with reference values derived from the rating curve (Q_{rc}) and the error was computed as

$$E_n = \frac{Q_n - Q_{rc}}{Q_{rc}}. \quad (12)$$

For each survey, two values of Q_2 were computed, reflecting the two possible choices of velocity values (odd-numbered or even-numbered transverse locations) and, analogously, three values of Q_3 were obtained. Figure 6 shows the variation of error with reference discharge. Overall, a two or three fold increase in transverse spacing has a moderate effect on discharge estimates, as errors increase by only a few percent with respect to those computed for the complete survey, and never exceed 10%.

A more detailed analysis of factors contributing to discharge uncertainty was performed using the uncertainty propagation method proposed by *Le Coz et al.* [2012, 2015]. This method (Q+) builds on the traditional uncertainty propagation approach of the ISO748 standard, with the following modified equation for gauged discharge uncertainty, $u(Q)$:

$$u^2(Q) = u_s^2 + u_{B,D}^2 + u_p^2 + u_{md}^2 + u_{mv}^2 + u_{c,e}^2, \quad (13)$$

where relative standard-uncertainty components, $u(X)$ in % of measured X , arise from residual systematic errors after best calibration of instruments (u_s), random errors in width and depth measurements ($u_{B,D}$), the limited number of point velocity measurements per vertical (u_p), the limited number and the position of the verticals used in the transverse integration of depths (u_{md}) and velocities (u_{mv}), and current-meter random errors and limited sampling time ($u_{c,e}$). The total uncertainty due to transverse integration of unit discharges (u_m^2) can be formed as

$$u_m^2 = u_{md}^2 + u_{mv}^2. \quad (14)$$

The main evolution from the ISO748 method is that both components of that important uncertainty component are estimated by considering the maximum variability of the transverse bed and velocity profiles between the verticals. This is achieved using an estimate of the transverse slope angle, which is specific to the geometry and nature of the bed. *Despax et al.* [2016] analyzed more than 3000 velocity-area gaugings and showed that the discharge-weighted mean of the observed angles between the verticals is a reasonable value for this parameter.

The uncertainty analysis was applied to four surveys (referred to as A, D, O, T, see Table 3) of the Adige River at San Lorenzo, covering the whole range of measured discharges and repeated using complete surveys, 1/2 and 1/3 of verticals. Based on the cross-sectional profile, the average transverse slope angle was assumed to be 2°. Table 3 summarizes the final expanded uncertainties and the relative contributions of distinct uncertainty sources to the total variance. The uncertainty budget is almost fully covered by the contributions of three main factors, namely i) errors associated with the choice of the velocity coefficient (term u_p); ii) errors due to the limited transverse resolution of velocity profiles (u_{mv}) and of the geometry data (u_{md}); and iii) systematic errors after best calibration of instruments (u_s , not shown in Table 3).

The final uncertainties considerably increase (from 5–6% on Q_1 to 9–16% on Q_3) when the number of SVR positions is reduced. The errors associated with the velocity coefficient remain dominant in the uncertainty budget for almost all cases (typically 60–80% of the total variance). The transverse integration errors clearly increase their contributions with a smaller number of SVR measurements, but more through the transverse resolution of the geometry profile than of the velocity. Using a more detailed bathymetry survey for computing the panel areas (as suggested by *Le Coz et al.* [2012]) would allow reducing the u_{md} component and hence the u_m .

These results suggest that it is possible to obtain an acceptable estimation of discharge with a small number of SVR positions across a section, at least in cross sections with sufficiently homogeneous depths and velocities like the San Lorenzo study case. Less detailed SVR surveys require shorter measurement time

Table 3. Uncertainty Estimates of four SVR Gaugings (A, D, O, T) of the Adige River at San Lorenzo and Percentage of Total Variance Due to the Number of Verticals Used to Compute Area (u_{md}), Velocity (u_{mv}), and Eventually Discharge (u_m) and Due to the Velocity Coefficient (u_p). Expanded Discharge Uncertainty is Computed for a 95% Level of Confidence

SVR Gauging	Number of SVR Verticals	Discharge (m ³ /s)	Expanded Discharge Uncertainty (2u) (%)	u_{md}^2/u^2 (%)	u_{mv}^2/u^2 (%)	u_m^2/u^2 (%)	u_p^2/u^2 (%)
A: Q ₁	15	437.6	4.9	1.6	0.4	2.0	81.4
A: Q ₂	8	432.9	6.9	6.3	1.5	7.8	80.0
A: Q ₃	4	410.9	10.5	21.0	4.4	25.5	67.6
D: Q ₁	12	71.9	5.8	7.7	2.0	9.7	67.8
D: Q ₂	6	68.2	9.4	24.1	6.6	30.7	59.1
D: Q ₃	3	69.8	16.0	50.8	11.4	62.2	33.1
O: Q ₁	8	1165.5	6.2	2.2	0.5	2.7	82.0
O: Q ₂	4	1140.0	9.1	8.3	1.8	10.0	82.1
O: Q ₃	2	1234.3	12.0	21.6	3.3	25.0	69.0
T: Q ₁	15	954.4	4.7	0.7	0.2	0.8	80.4
T: Q ₂	8	943.1	6.4	2.7	0.7	3.4	81.7
T: Q ₃	4	923.0	9.4	8.9	2.3	11.2	80.0

windows, which are crucial to obtain reliable discharge estimation under rapidly changing flow conditions (such as flash floods) or to perform discharge measurements at multiple cross sections in a catchment during flood conditions.

5. Discussion

5.1. Guidelines for SVR Deployment

Tests presented in this paper show that handheld surface velocity radars are highly versatile instruments that can be safely used for stream gauging in a wide variety of riverine contexts. Unlike most conventional instrumentation, SVR surveys require minimal training, equipment and manpower. In most cases, a single person is sufficient and recent tests carried out on the Rhône River showed that nonspecialist operators can successfully use an SVR device after a 1 hour training. Ease-of-use and limited costs open new possibilities for large-scale flood monitoring, including deployment by trained local residents on behalf of river authorities in remote areas.

However, optimal use of SVR devices requires careful selection of gauging sites, operational parameters (such as deployment position, tilt angle and transverse resolution along the cross section) and weather conditions. As handheld radars do not provide information on cross-section shape, the availability and quality of cross-sectional data is a major factor in the selection of gauging sites. *Le Coz et al.* [2012] showed that bathymetry interpolation using additional verticals can significantly improve discharge estimates. However, geometry data are usually acquired at low flow before or after floods and thus errors in discharge estimation due to bed change during floods may occur. Simultaneous, noncontact velocity and GPR bathymetry surveys have been carried out [*Cheng et al.*, 2004; *Costa et al.*, 2006; *Haeni et al.*, 2000; *Melcher et al.*, 2002], but low-cost, real-time surveying of a river bed under high flows remains an open challenge.

Gauging sections with bridges perpendicular to the flow are preferable, as no yaw angle correction is needed and resulting velocity values are averaged over areas of equal size along the transect. However, accurate discharge estimates have also been obtained from banks (at Venzone) and similar outcomes are reported in the literature [see e.g., *Costa et al.*, 2000, 2006]. Projection error can be estimated using a formulation similar to that proposed by *Tamari et al.* [2014]. Deployment from very high bridges and/or a low tilt angle result in large distances between the antenna and the target, which, in turn, produce large illuminated areas and a weaker return signal. Spatial averaging over large areas filters out local disturbances of the velocity field, improving the accuracy of discharge estimation, but can also result in an oversimplification of the transverse velocity profile and, thus, in poor discharge estimates. The latter case was observed for the Braulins cross sections, where measurements were taken from a 10 m high bridge and the illuminated area covered the whole channel width. High free surface roughness is particularly important to ensure reliable velocity measurements over long distances [*Decatur Electronics*, 2011]. In the present set of experiments, stable and accurate readings were obtained for distances up to 50 m even under low turbulence conditions, suggesting that the SVR operational range can extend to several tens of meters.

In case of insufficient return signal strength, it is advisable to increase tilt angle above 30° and up to 60° and to ensure high free surface roughness. However, a large tilt angle also decreases accuracy because the velocity component perpendicular to the antenna is small. Systematic underestimation of velocity has been reported by *Tamari et al.* [2013] for tilt angles larger than $45\text{--}55^\circ$. Moreover, tiltmeter inaccuracy was found to affect velocity accuracy with systematic errors up to 10%.

The number of cross-sectional positions for SVR measurements determines the transverse resolution of the velocity profile but also the duration of the survey. For example, a complete survey of the 80 m wide San Lorenzo cross section in the Adige River requires approximately 40 minutes for a 5.7 m spacing and 20 minutes for a 17.1 m spacing. Both survey duration and spacing can affect the accuracy of discharge estimates, although errors in large rivers such as the Adige can be as low as 5% even with a small number of cross-sectional positions (see Figure 6). Survey duration is particularly important to gauge rapidly changing high flow conditions. Uncertainty analysis tools [*Le Coz et al.*, 2012, 2015] allow comparison of integration errors due to these components and can therefore help to optimize the measurement field procedures. An estimation of uncertainty due to flow unsteadiness was computed for the San Lorenzo section using the formulation proposed by *Le Coz et al.* [2012] with a level of confidence of 95%. The highest discharge values gauged at this site were obtained from seven verticals with an 11.4 m spacing acquired over a 30 min window. During the measurement, discharge slowly increased from about 1060 to 1130 m^3/s , resulting in an uncertainty of 3.6%.

In contrast, rapid flow variations occur on the Noce River at Pellizzano because of hydropeaking, with discharge typically increasing from about 3 to 11 m^3/s within 15 minutes. In this case, a 15 min long measurement carried out during the rising phase would yield an error of 66%. These examples show the potential of SVR to gauge unsteady flow conditions, where short measurement time windows are crucial to minimize uncertainty. While limited information is available in the literature about average gauging times under flood conditions, *Costa et al.* [2006] report that more than two hours are needed for a conventional survey with contact instruments under high flow in a 100 m wide river.

Finally, weather conditions also influence SVR readings. In particular, precipitation can disrupt surveys and erratic readings have been observed under light rain. Also, wind can influence the shape of the velocity profile close to the surface and produce spurious waves [see *Costa et al.*, 2006; *Plant et al.*, 2005]. An attempt to quantify the influence of wind on surface water velocity was made during steady flow velocity surveys on the Ein Fesh'ha. Wind was almost parallel to flow direction with an average velocity of 4.4 m/s and a maximum of 8.6 m/s. Despite variations in wind speed, water surface velocity remained constant at 0.7 m/s. However, no systematic testing of wind effect was performed at other sites. Rather, care was taken in avoiding rain and strong wind conditions during surveys.

5.2. Choice of Velocity Coefficient

As shown in Table 3, the choice of the velocity coefficient is the key factor in SVR-based discharge estimates. The default value of α derives from the assumption of a logarithmic distribution of velocity along the vertical, and the validity of this hypothesis strongly depends on relative roughness and flow uniformity. Therefore, the relationship between α and relative roughness was explored in detail by exploiting the wide range of flow conditions observed across the study sites.

Velocity distributions are well approximated by a logarithmic law over much of the flow depth in smooth and rough bed streams, but not in the presence of local features such as bridge piers, bars and debris [*Smart*, 1999]. Large spatial heterogeneities of the bed in shallow channels (such as anabranches of the braided Tagliamento River) likely have a similar effect on the velocity profile. Moreover, approximately a quarter of the computed α values are larger than one, implying that depth-averaged velocity is larger than surface velocity. This is impossible under the assumption of a monotonous velocity distribution along the vertical coordinate and may indicate that the maximum velocity occurs below the surface (velocity dip phenomenon). This effect has often been attributed to secondary currents, but velocity distributions close to the surface are still poorly understood in comparison with near-bed processes. Extreme values of the velocity coefficient can also be a product of spatial averaging. Very low values of α are observed close to the banks, where depth-averaged velocities obtained from contact measurements are much lower than the corresponding, SVR-derived surface velocities. In this case, large illuminated areas may include high-velocity areas closer to the section center, thus explaining unusually high surface velocities.

Interestingly, the variability of global (cross-section averaged) values of α is considerably smaller than that of local values of α . Moreover, extreme values (outside the 1st–9th percentile range) occur for relative roughness values larger than 0.02 in the case of local α , as opposed to 0.07 for global α . This implies that spatial averaging, which filters out local oscillations caused by turbulence and local changes in cross-sectional morphology, can be beneficial when gauging shallow flows, where the velocity coefficient shows the largest variability if computed at local scale. These results clearly suggest that the handheld radars are likely more suited for global measurements of discharge rather than local velocity estimates. However, care must be taken in comparing conventional contact measurements with SVR gaugings, as the radar intrinsically filters out small-scale variations because of spatial averaging over the illuminated area. Comparisons with published data show similar results. For example, *Lee and Julien* [2006] report a larger variability (0.42–0.77) of local α values in a shallow gravel bed river as compared to a deeper, clay bed canal (0.68–0.94). The global velocity coefficient for the two sites is 0.61 and 0.79, respectively, and these values are in good agreement with those shown in Figure 4. Moreover, global α values obtained in smoother channels (relative roughness smaller than 0.07) almost always fall into the range proposed in ISO 748 (0.80–0.91, average 0.86), further confirming that standardized procedures can safely be applied in these channels.

Results proposed in this study show that discharge estimation obtained with the widely used default α (0.85) are accurate within 10% if relative roughness is lower than approximately 0.01. Therefore, the default value of the velocity coefficient is acceptable for deep, hydrodynamically smooth channels where the assumption of a logarithmic velocity profile is sufficiently consistent with field conditions. Similar results were obtained by *Le Coz et al.* [2010] for LSPIV surface velocity data on the low-roughness Saone River. While the authors show that the velocity profile is best approximated by a piecewise logarithmic-constant distribution, they also note that the resulting velocity coefficient is within 10% of the default value. In contrast, error in rough streams can be as high as 30% and therefore a calibrated velocity coefficient is needed in this case to ensure accurate discharge estimation.

5.3. Application of SVR for the Extension/Validation of Rating Curves

The case study of the Adige River at the San Lorenzo station is a good example of the use of SVR gaugings for the extension and validation of rating curves in high discharge conditions. Nonintrusive devices are easy to deploy and often make it possible to produce discharge data for floods that were either scarcely or never previously documented. Surface velocity radars can be more uncertain than conventional intrusive methods because of the limited knowledge of the bed changes and of the value of the velocity coefficient. However, discharge estimates from rating curves also rely on geometry data acquired at low flows before or after floods. Moreover, SVR measurements can be more accurate than conventional surveys during flash floods, as the shorter duration of field operations allows to capture rapid discharge changes. As shown by this example, even if a larger uncertainty is considered for SVR gaugings, they can supply enough information to considerably reduce the uncertainty in the extension of most of the existing rating curves for high flows.

Figure 7 shows SVR-based discharge measurements for the San Lorenzo station on the Adige River (70–1100 m³/s) and the official rating curve provided by the Adige River Basin Authority. This rating curve is based on a large database of ADCP/current meter measurements covering the range 50–500 m³/s. Within this range, our SVR-based gaugings are in good agreement with ADCP data and with the rating curve. However, at higher flows SVR estimates are up to 10% lower than discharge values computed from the rating curve extrapolation.

To answer the question of how significant is this deviation, a Bayesian analysis of the rating curve and the associated uncertainties was conducted using the BaRatin approach [*Le Coz et al.*, 2014]. This approach combines user-defined prior knowledge on the hydraulic controls and gaugings that come with their individual uncertainties. Default uncertainty values were assigned to gaugings at the 95% level of confidence: $\pm 5\%$ for ADCP/current meter discharges since they were measured in favorable conditions; $\pm 7\%$ for SVR discharges assuming the standard deviation of global α for smooth channels ($d_{50}/D_m \leq 0.05$; see chapter 4.1.3).

In the case of the Adige River at San Lorenzo, two types of hydraulic controls can be identified from photographs of different flow conditions: at low flows, a complex critical section formed by natural riffles; at medium and high flows, the embanked main channel. In BaRatin, the two controls are represented by a horizontal weir and a uniform flow within a wide, rectangular channel, respectively. The results obtained from BaRatin (cf. Figure 7) show that adding the SVR data to the existing gaugings significantly changes the

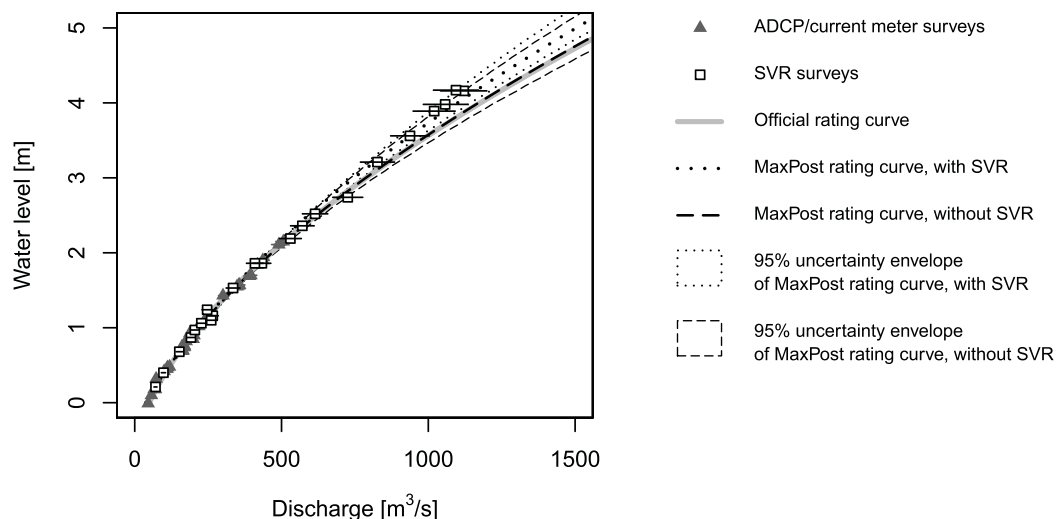


Figure 7. The Adige River at San Lorenzo, Italy: conventional and SVR gauging data with their uncertainty bars; official rating curve (grey line); MaxPost rating curves and their associated 95% uncertainty envelopes as obtained using the BaRatin Bayesian approach, with or without SVR data.

upper end of the rating curve and reduces its uncertainty interval. The uncertainty bars of all gaugings are included in the uncertainty envelope of the rating curve, suggesting that the two identified controls are a reasonable prior assumption for this hydrometric station. Such results are particularly decisive for establishing streamflow records above the highest observed data.

6. Conclusions

We report on extensive testing of a portable surface velocity radar, a non-contact gauging technique that allows discharge estimation under high flow conditions. The applicability of radar velocimetry for stream gauging was evaluated through a series of field-scale experiments carried out in a variety of riverine contexts, from high roughness mountain streams to large piedmont rivers. Radar-derived velocity profiles and discharge estimates were compared with data obtained from conventional techniques (including ADCP, current meters and floats), as well as LSPIV and official rating curves.

Comparisons show that velocity profiles match contact measurements, with larger uncertainties close to the banks ascribed to local disturbances of the flow such as secondary currents and eddies. Discrepancies are also caused by different space averaging of velocity values, but this error affects only a small portion of the cross section.

Discharge was computed from SVR surveys by defining a velocity coefficient α , which represents the ratio of depth-averaged to surface velocity values. The coefficient α was computed experimentally from noncontact and conventional velocity surveys and compared with theoretical formulations for the vertical velocity profiles and standard values reported in the literature. The velocity coefficient shows large fluctuations if computed on individual verticals, especially in high roughness channels where the vertical velocity profile is not expected to follow a logarithmic distribution. In contrast, cross-section averaged values of α are more stable and in good agreement with theoretical values. Our findings show that the widely used standard value of α (0.85) is a valid choice over a wide range of roughness values. However, its use can lead to an underestimation of discharge in very smooth channels and an overestimation of discharge in rough channels. In these cases, a site-specific calibration of α on the basis of simultaneous contact and noncontact measurements is to be preferred.

Overall, SVR-based discharge estimates are accurate within 10% for intermediate roughness flows, while larger errors are observed at very low relative roughness (< 0.05). Moreover, accuracy does not strongly depend on the cross-sectional spacing of SVR points, implying that SVR can be used to gauge unsteady flow conditions. Finally, we show that noncontact devices can be used to extend the range of validity of rating curves by providing much-needed direct information on water velocity at high flows, especially so in flashfloods.

Acknowledgments

We wish to acknowledge the contribution to measurements from many operators of Irstea (especially Mickaël Lagouy, Fabien Thollet, Raphaël Le Boursicaud), EDF, CNR (especially Thierry Pantel), DREAL Rhône-Alpes (especially Patrick Duby). We also wish to thank the staff of the Servizio Idrografico of the Regione Friuli Venezia Giulia, the Ufficio Dighe of the Autonomous Province of Trento and the Ufficio Idrografico of the Autonomous Province of Bolzano for their collaboration. Dolomiti Edison Energy provided data for the Mezzocorona power plant site. SVR surveys in Italy were performed by Fabio Piazza, Elena Bastianon, Francesca La Torre, Francesco Martinolli, Elena Nucci, Massimiliano Scapini, Alessandro Zorzin and Fabiano Carolli, with the help of Mauro Carolli, Guglielmo Stecca, Marco Redolfi, Marco Tubino and Walter Bertoldi. The SVR measurements in Israel were performed by Yuval and Nava Lorig, Dror Paz, Nir Fridman, with help by Yaniv Munwes, Yael Storz-Peretz, Noa Hillel, Ronel Barzilai and Alon Yaron. Special thanks to Yehoshua Ratzon for technical assistance. We thank Aurélien Despax for applying the uncertainty analysis to San Lorenzo SVR gaugings. This study was partially supported by a PhD grant of the University of Trento and by a grant of APRIE (Agenzia Per le Risorse Idriche e l'Energia) of the Autonomous Province of Trento. This study was also supported by the French national hydrological services (SCHAPI). The FloodScale project is funded by the French National Research Agency (ANR) under contract ANR 2011 B556 027 01, which contributes to the HyMeX program. The SUMAR and DESERVE projects were funded by the German Federal Ministry of Education and Research (BMBF) and the Helmholtz Association, with particular help by Stefan Geyer. The Israel Science Foundation funded measurements in the Eshtemoa under contract No ISF1073/09. D. Zamler received scholarships from the Israel Water Authority and the Ben Gurion University of the Negev. We thank the Associate Editor, Tommaso Moramarco and two anonymous reviewers for their thorough and insightful reviews of the manuscript. Primary stream gauging data used in this paper are available from the authors upon request (mwelber@uwo.ca).

References

- Chen, Y. C., and C. L. Chiu (2004), A fast method of flood discharge estimation, *Hydrol. Processes*, 18(9), 1671–1684.
- Cheng, R. T., J. W. Gartner, R. R. Mason, J. E. Costa, W. J. Plant, K. R. Spicer, F. P. Haeni, N. B. Melcher, W. C. Keller, and K. Hayes (2004), Evaluating a radar-based, non contact streamflow measurement system in the San Joaquin River at Vernalis, California, *U.S. Geol. Surv. Open-File Rep.* 04-1015, 16 pp.
- Chiu, C. L., Hsu, S. M. and N. C. Tung (2005), Efficient methods of discharge measurements in rivers and streams based on the probability concept, *Hydrol. Processes*, 19, 3935–3946.
- Corato, G., T. Moramarco, and T. Tucciarelli (2011), Discharge estimation combining flow routing and occasional measurements of velocity, *Hydrol. Earth Syst. Sci.*, 15(9), 2979–2994.
- Costa, J. E., K. R. Spicer, R. T. Cheng, P. F. Haeni, N. B. Melcher, E. M. Thurman, W. J. Plant, and W. C. Keller (2000), Measuring stream discharge by non-contact methods: A proof-of-concept experiment, *Geophys. Res. Lett.*, 27(4), 553–556.
- Costa, J. E., R. T. Cheng, F. P. Haeni, N. Melcher, K. R. Spicer, E. Hayes, W. Plant, K. Hayes, C. Teague, and D. Barrick (2006), Use of radars to monitor stream discharge by noncontact methods, *Water Resour. Res.*, 42, W07422, doi:10.1029/2005WR004430.
- Decatur Electronics (2011), *SVR(TM) User's Manual, Rev 2.*, Decatur, Ill.
- Despax, A., Perret, C., Garçon, R., Hauet, A., Belleville, A., Le Coz, J., Favre, A. C. (2016), Considering sampling strategy and cross-section complexity for estimating the uncertainty of discharge measurements using the velocity-area method, *J. Hydrol.*, 533, 128–140.
- Dittrich, A., and K. Koll (1997), Velocity field and resistance of flow over rough surfaces with large and small relative submergence, *Int. J. Sediment Res.*, 12(3), 21–33.
- Dramais, G., J. Le Coz, B. Camenen, and A. Hauet (2011), Advantages of a mobile LSPIV method for measuring flood discharges and improving stage–discharge curves, *J. Hydro-environ. Res.*, 5(4), 301–312.
- Engelund, F., and E. Hansen (1967), *A Monograph on Sediment Transport in Alluvial Streams*, Teknisk Forlag, Copenhagen.
- Fujita, I., H. Watanabe, and R. Tsubaki (2007), Development of a non-intrusive and efficient flow monitoring technique: The space-time image velocimetry (STIV), *Int. J. River Basin Manage.*, 5(2), 105–114.
- Fukami, K., T. Yamaguchi, H. Imamura, and Y. Tashiro (2008), Current status of river discharge observation using non-contact current meter for operational use in Japan, *World Environmental and Water Resources Congress 2008*, pp. 1–10, Ahupua'a, Hawaii.
- Fulton, J., and J. Ostrowski (2008), Measuring real-time streamflow using emerging technologies: Radar, hydroacoustics, and the probability concept, *J. Hydrol.*, 357(1), 1–10.
- Haeni, F. P., M. L. Buursink, J. L. Costa, N. B. Melcher, R. T. Cheng, and W. J. Plant (2000), Ground-Penetrating RADAR Methods used in surface-water discharge measurements, in *GPR 2000—Proceedings of the Eighth International Conference on Ground Penetrating Radar, Gold Coast, Australia, SPIE - The International Society for Optical Engineering*, edited by D. A. Noon, G. F. Stickley, and D. Longstaff, pp. 494–500, Univ. of Queensland, Queensland, Australia, doi:10.1117/12.383618.
- ISO (2007), *Hydrometry — Measurement of liquid flow in open channels using current-meters or floats*, BSI.
- Jendzurski, J., and N. G. Paulter (2009), Calibration of speed enforcement down—The road radars, *J. Res. Natl. Inst. Stand. Technol.*, 114(3), 137–148.
- Kawanisi, K., M. Razaz, K. Ishikawa, J. Yano, and M. Soltaniasl (2012), Continuous measurements of flow rate in a shallow gravel-bed river by a new acoustic system, *Water Resour. Res.*, 48, W05547, doi:10.1029/2012WR012064.
- Lassabatere, L., J. H. Pu, H. Bonakdari, C. Joannis, and F. Larrarte (2012), Velocity distribution in open channel flows: Analytical approach for the outer region, *J. Hydraul. Eng.*, 139(1), 37–43.
- Le Coz, J., A. Hauet, G. Pierrefeu, G. Dramais, and B. Camenen (2010), Performance of image-based velocimetry (LSPIV) applied to flash-flood discharge measurements in Mediterranean rivers, *J. Hydrol.*, 394(1–2), 42–52.
- Le Coz, J., B. Camenen, X. Peyrard, and G. Dramais (2012), Uncertainty in open-channel discharges measured with the velocity-area method, *Flow Meas. Instrum.*, 26, 18–29.
- Le Coz, J., B. Renard, L. Bonnifait, F. Branger, and R. Le Boursicaud (2014), Combining hydraulic knowledge and uncertain gaugings in the estimation of hydrometric rating curves: A Bayesian approach, *J. Hydrol.*, 509, 573–587.
- Le Coz, J., B. Camenen, X. Peyrard, and G. Dramais (2015), Erratum to “Uncertainty in open-channel discharges measured with the velocity-area method [Flow Meas. Instrum. 26 (2012) 18–29]”, *Flow Meas. Instrum.*, 46, 193–194.
- Lee, J. S., and P. Y. Julien (2006), Electromagnetic wave surface velocimetry, *J. Hydraul. Eng.*, 132(2), 146–153.
- Lee, M. C., J. M. Leu, C. J. Lai, W. J. Plant, W. C. Keller, and K. Hayes (2002), Non-contact flood discharge measurements using an X-band pulse radar (II) Improvements and applications, *Flow Meas. Instrum.*, 13(5–6), 271–276.
- Melcher, N. B., et al. (2002), River discharge measurements by using helicopter-mounted radar, *Geophys. Res. Lett.*, 29(22), 2084, doi: 10.1029/2002GL015525.
- Muste, M., I. Fujita, and A. Hauet (2008), Large-scale particle image velocimetry for measurements in riverine environments, *Water Resour. Res.*, 44, W00D19, doi:10.1029/2008WR006950.
- Nikora, V., D. Goring, I. McEwan, and G. Griffiths (2001), Spatially averaged open-channel flow over rough bed, *J. Hydraul. Eng.*, 127(2), 123–133.
- Nikora, V., S. McLean, S. Coleman, D. Pokrajac, I. McEwan, L. Campbell, J. Aberle, D. Clunie, and K. Koll (2007), Double-averaging concept for rough-bed open-channel and overland flows: Applications, *J. Hydraul. Eng.*, 133(8), 884–895.
- Plant, W. J., W. C. Keller, and K. Hayes (2005), Measurement of river surface currents with coherent microwave systems, *IEEE Trans. Geosci. Remote Sens.*, 43(6), 1242–1257.
- Rantz, S. (1982), Measurement and computation of stream flow. Volume 1: Measurement of stage and discharge; Volume 2: Computation of discharge, *U.S. Geol. Surv. Water Supply Pap.*, 2175, 631.
- Smart, G. M. (1999), Turbulent velocity profiles and boundary shear in gravel bed rivers, *J. Hydraul. Eng.*, 125(2), 106–116.
- Tamari, S., F. García, J. I. Arciniega-Ambrocio, and A. Porter (2013), *Laboratory and Field Testing of a Handheld Radar to Measure the Water Velocity at the Surface of Open Channels*, Inst. Mexicano de Tecnología del Agua, Secretaría de Medio Ambiente y Recursos Naturales, Jiutepec, Morelos, Mexico.
- Tamari, S., F. García, J. I. Arciniega-Ambrocio, and A. Porter (2014), Testing a handheld radar to measure water velocity at the surface of channels, *La Houille Blanche*, 3, 30–36.
- Teague, C. C., D. E. Barrick, P. Lilleboe, and R. T. Cheng (2001), Canal and river tests of a riversonde measurement system, in *Proceedings IEEE 2001 International Geoscience and Remote Sensing Symposium*, pp. 1288–1290, Institute of Electrical and Electronics Engineers (IEEE), Sydney, Australia.
- Wang, X., Z. Wang, M. Yu, and D. Li (2001), Velocity profile of sediment suspensions and comparison of log-law and wake-law, *J. Hydraul. Res.*, 39(2), 211–217.
- Yorozuya, A., Y. Kanno, K. Fukami, and K. Oodaira (2010), Development of automatic water discharge measurement system, in *6th International Symposium on Environmental Hydraulics*, Taylor and Francis, London, U. K.